Hindawi Publishing Corporation
Mathematical Problems in Engineering
Volume 2016, Article ID 1713046, 9 pages
http://dx.doi.org/10.1155/2016/1713046

*Research Article*

# Time-Frequency Analysis Based on Improved Variational Mode Decomposition and Teager Energy Operator for Rotor System Fault Diagnosis

**Shangkun Liu, Guiji Tang, Xiaolong Wang, and Yuling He**

*School of Energy, Power and Mechanical Engineering, North China Electric Power University, Baoding 071000, China*

Correspondence should be addressed to Shangkun Liu; lsk1213@163.com

Received 12 July 2016; Revised 21 September 2016; Accepted 13 October 2016

Academic Editor: Zhike Peng



A time-frequency analysis method based on improved variational mode decomposition and Teager energy operator (IVMD-TEO) is proposed for fault diagnosis of turbine rotor. Variational mode decomposition (VMD) can decompose a multicomponent signal into a number of band-limited monocomponent signals and can effectively avoid model mixing. To determine the number of monocomponents adaptively, VMD is improved using the correlation coefficient criterion. Firstly, IVMD algorithm is used to decompose a multicomponent signal into a number of monocompositions adaptively. Second, all the monocomponent signals' instantaneous amplitude and instantaneous frequency are demodulated via TEO, respectively, because TEO has fast and high precision demodulation advantages to monocomponent signal. Finally, the time-frequency representation of original signal is exhibited by superposing the time-frequency representations of all the monocomponents. The analysis results of simulation signal and experimental turbine rotor in rising speed condition demonstrate that the proposed method has perfect multicomponent signal decomposition capacity and good time-frequency expression. It is a promising time-frequency analysis method for rotor fault diagnosis.

## 1. Introduction

The fault vibration signal of turbine and other larger-scale rotating machinery is often characterized by multicomponent and nonstationary on account of large span, complex structure, and variable working condition. Time-frequency analysis method can provide nonstationary signal's localization information both in time domain and in frequency domain, so it has been widely used in rotating mechanical fault diagnosis [1–10]. The key of time-frequency analysis is to find an effective method to decompose the multicomponent signal. Aiming at this problem, scholars have carried on unceasing exploration. Li and Liang used the generalized synchrosqueezing transform to detect and diagnose faults of the gearbox through analyzing the time-frequency representation [2]. Feng et al. proposed the iterative generalized synchrosqueezing transform to diagnose the lab experimental vibration signals of planetary gearboxes under nonstationary conditions [3]. A time-frequency analysis method based on the Vold-Kalman filter and higher-order energy separation was proposed by Feng et al., and it was used to diagnose the planetary gearbox fault under varying shaft speed [4]. The cracked rotor transient response was analyzed and monitored using HHT by Ramesh Babu et al. [5]. Liu et al. diagnosed the rotor rub-impact fault using Teager Huang transform [6], but these methods based on Empirical Mode Decomposition (EMD) had the problems of mode mixing, over envelope, less envelope, and so forth [7, 8], which affected the analysis results. Chandra and Sekhar found that Continuous Wavelet Transform (CWT) was more preferred than HHT for noisy data and it was valid to diagnose the shaft misalignment and rotor stator rub-impact faults [8]. Li et al. distinguished the severity degree of rub-impact fault using Empirical Wavelet Transform (EWT) [9]. Tang and Pang extracted the typical fault characteristics of oil-whirl using Hilbert vibration decomposition (HVD) [10].

Dragomiretskiy and Zosso proposed a new multicomponent signal decomposition method called variational mode

decomposition (VMD) [11]. This method can decompose a multicomponent signal into a given number of band-limited intrinsic mode functions using frequency domain nonrecursive iteration pattern. VMD has high precision and can effectively avoid the problem of mode mixing [12]. It has better performance than EWT to produce the classification feature vectors of power quality disturbances [13]. Wang et al. found that the filtering characteristic of VMD was wavelet packet-like expansion via numerical simulations and used it to analyze the fixed frequency rotor rub-impact fault in time domain [14]. However, how to select the appropriate parameter of VMD, especially the number of decomposed components, is very important in practice. To solve this problem, the IVMD which uses the correlation coefficient criterion to determine the number of components adaptively is applied in this paper. Combining the fast and high precision advantages of TEO to monocomponent signal, an IVMD-TEO time-frequency analysis new method is proposed. The analysis results of simulation signal and experiment turbine rotor fault signal illustrate the effect of this method.

## 2. IVMD-TEO Time-Frequency Analysis Method

*2.1. Theory of VMD.* For a multicomposition real valued signal $f$, VMD assumes that $f$ is composed of a given number of subsignals $u_k$ (modes). Each mode is regarded as an amplitude-modulated and frequency-modulated (AM-FM) signal and has mostly compact frequency $\omega_k$ around a center pulsation. These modes are called intrinsic mode functions (IMFs). The constrained variational problem is the following:

$$\begin{aligned} \min_{\{u_k\},\{\omega_k\}} \quad & \left\{ \sum_k \left\| \partial_t \left[ \left( \sigma(t) + \frac{j}{\pi t} \right) * u_k(t) \right] e^{-j\omega_k t} \right\|_2^2 \right\} \\ \text{s.t.} \quad & \sum_k u_k(t) = f. \end{aligned} \tag{1}$$

To assess the bandwidth of the modes, the following scheme is proposed. (1) Compute the associated analytic signal by means of the Hilbert transform to obtain a unilateral frequency spectrum for each mode. (2) Shift the frequency spectrum of each mode to the baseband by mixing with an exponential tuned to the estimated center frequency. (3) Estimate the bandwidth through the $H^1$ Gaussian smoothness of the demodulated signal, that is, the squared $L^2$-norm of the gradient [11].

To solve the constrained variational problem, the augmented Lagrangian is introduced and the nonconstrained variational problem is gotten by

$$\begin{aligned} & L\left(\{u_k\},\{\omega_k\},\lambda\right) \\ & \quad = \alpha \sum_k \left\| \partial_t \left[ \left( \sigma(t) + \frac{j}{\pi t} \right) * u_k(t) \right] e^{-j\omega_k t} \right\|_2^2 \\ & \quad + \left\| f(t) - \sum_k u_k(t) \right\|_2^2 \\ & \quad + \left\langle \lambda(t), f(t) - \sum_k u_k(t) \right\rangle, \end{aligned} \tag{2}$$

where $\alpha$ denotes the balancing parameter of the fidelity constraint. The saddle point of (2) is the optimal solution of original problem, which can be gained using alternate direction method of multipliers (ADMM) [15]. All the modes can be obtained from (3) in the frequency domain through updating each mode and its center frequency $\omega_k$ constantly:

$$\hat{u}_k^{n+1}(\omega) = \frac{\hat{f}(\omega) - \sum_{i \neq k} \hat{u}_i(\omega) + \hat{\lambda}(\omega)/2}{1 + 2\alpha\left(\omega - \omega_k\right)^2}. \tag{3}$$

$\hat{u}_k^{n+1}$ is regarded as the Wiener filtering result of the residue $\hat{f}(\omega) - \sum_{i \neq k} \hat{u}_i(\omega)$, which makes the VMD algorithm much more robust to sampling and noise. The new center frequency $\omega_k^{n+1}$ is put at the center of gravity of the corresponding mode's power spectrum, which can be updated by

$$\omega_k^{n+1} = \frac{\int_0^\infty \omega \left|\hat{u}_k(\omega)\right|^2 d\omega}{\int_0^\infty \left|\hat{u}_k(\omega)\right|^2 d\omega}. \tag{4}$$

*2.2. Improved VMD.* It is known from VMD algorithm that the number of decomposed components $K$ must be set in advance. However, the $K$ value is usually difficult to be accurately set for different conditions. In order to solve this problem, the correlation coefficient criterion is introduced to control the number $K$ adaptively in this paper, named IVMD.

The correlation coefficient is a quantitative measure of correlation and dependence. It shows the statistical relationships between two or more random variables or observed data values. It has been used in the chromosomes' similarity analysis [16], the relationship analysis between cerebral venous thrombosis and oral contraceptives in adult women [17], and the mechanical vibration signal similarity analysis [18, 19]. In this paper, Pearson's correlation coefficient is used and can be measured by

$$r(X,Y) = \frac{\operatorname{cov}(X,Y)}{\sigma_X \sigma_Y}, \tag{5}$$

where $r(X,Y)$ is the correlation coefficient of $X$ and $Y$, $\operatorname{cov}(X,Y)$ is the covariance between $X$ and $Y$, and $\sigma_X$ and $\sigma_Y$ are standard deviations of $X$ and $Y$.

The correlation coefficient between the decomposed residue of VMD and original signal is computed by (5). When the absolute value is lower than the threshold (0.05 in this paper), it is thought that there is not important information in the residue and the original signal is decomposed completely and appropriately. The iterative decomposition process is finished, and the number $K$ can be determined adaptively.

The implementation steps of IVMD are as follows:

(1) initial: $K = 1$;

(2) $\mathrm{Do}_1$: $K = K + 1$;

(3) initial: $\{\widehat{u}_k^1\}, \{\widehat{\omega}_k^1\}, \widehat{\lambda}^1$ and $n$;

(4) $\mathrm{Do}_2$: $n = n + 1$;

(5) for $k = 1: K$, update $\widehat{u}_k^{n+1}$ and $\omega_k^{n+1}$ using (3) and (4), respectively;

(6) update $\widehat{\lambda}^{n+1}(\omega) \leftarrow \widehat{\lambda}^n(\omega) + \tau(\widehat{f}(\omega) - \sum_k \widehat{u}_k^{n+1}(\omega))$;

(7) $\mathrm{repeat}_2$ steps (4)–(6), until $\sum_k \|\widehat{u}_k^{n+1} - \widehat{u}_k^n\|_2^2 / \|\widehat{u}_k^n\|_2^2 < \varepsilon$;

(8) $\mathrm{repeat}_1$ steps (2)–(7), until $|r(f - \sum u_k, f)| < \delta$.

*2.3. Teager Energy Operator.* To express time-frequency representation of each mode, the demodulation analysis is necessary to each IMF. TEO is a kind of nonlinear local differential operator without involving integral transform. It can improve the estimation of the instantaneous spectrum characteristics of the vibration data under certain conditions [7]. It has been widely used in bearing fault diagnosis in recent years [20–22].

For the AM-FM signal $x(t) = a(t)\cos[\phi(t)]$, the corresponding TEO is defined as

$$\psi[x(t)] = [\dot{x}(t)]^2 - x(t)\,\ddot{x}(t), \tag{6}$$

where $\dot{x}(t)$ and $\ddot{x}(t)$ are its first and second derivatives, respectively. In the discrete time case, the time derivatives in (6) can be approximated to

$$\psi[x(n)] = x^2(n) - x(n+1)\,x(n-1). \tag{7}$$

TEO offers excellent time resolution and demodulation speed because only three sample points are required for the energy computation at each time instant. As a result, the instantaneous change in amplitude and frequency of signal can be quickly tracked. The AM and FM information of vibration signals can be extracted using, respectively [23],

$$a(n) = \frac{2\psi[x(n)]}{\sqrt{\psi[x(n+1) - x[n-1]]}}, \tag{8}$$

$$f(n) = \frac{1}{4\pi}\arccos\left[1 - \frac{\psi[x(n+1) - x(n-1)]}{2\psi[x(n)]}\right]. \tag{9}$$

*2.4. IVMD-TEO Time-Frequency Analysis Method.* Combining the advantages of IVMD and TEO, a time-frequency analysis method named IVMD-TEO is proposed in this paper. First of all, IVMD algorithm is used to decompose a multicomponent signal into $K$ IMFs adaptively. Then, the instantaneous amplitude and instantaneous frequency of each IMF are demodulated by TEO. Finally, the time-frequency representation of the original signal is obtained by superposing the time-frequency representations of all the monocomponents, and the fault types are diagnosed by analyzing the fault characteristic frequency components showed in the time-frequency representation diagram.

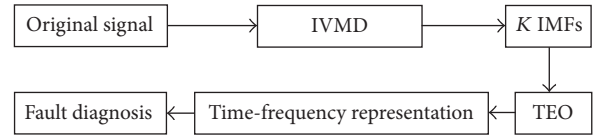


Figure 1: IVMD-TEO time-frequency analysis flow chart.

In the process of VMD, the balancing parameter $\alpha$ is a parameter to balance the fidelity. The bigger value is suitable to filter low-frequency component (e.g., trend term) and the smaller value is suitable to detect impacts from a time series (or signal) [24], so the smaller value ($\alpha = 500$) is used in this paper.

The time-frequency analysis process of the proposed IVMD-TEO method for rotor system is shown in Figure 1, and the specific implementation steps are as follows.

(1) Gather original signal data from experimental rotor rig or practical rotor system.

(2) Decompose the original signal (multicomposition) into a number of monocompositions ($K$ IMFs) by IVMD method adaptively.

(3) Demodulate the instantaneous amplitude and instantaneous frequency of each IMF using TEO.

(4) Draw the time-frequency representation diagram of original signal by superposing all time-frequency representations of monocomponents.

(5) Diagnose the rotor system fault types by observing the corresponding fault characteristic frequency components that appeared possibly in Figure 1.

## 3. Simulation Signal Analysis

$$\begin{aligned} x_1(t) &= \cos\left(2\pi 50t + 2\pi 20t^2\right) \\ &\quad + \cos\left(2\pi 90t + 2\pi 30t^2\right), \\ x_2(t) &= \begin{cases} \cos(2\pi 150t), & t < 0.3 \\ \cos(2\pi 180t), & t \geq 0.3, \end{cases} \\ x_3(t) &= [1 + 0.5\sin(2\pi 5t)]\cos(2\pi 210t), \\ x(t) &= x_1(t) + x_2(t) + x_3(t) + s(t). \end{aligned} \tag{10}$$

A multicomponent simulation signal $x(t)$ is used to verify the time-frequency analysis effect of the proposed method. $x(t)$ is composed of two FM components $x_1(t)$, two mutation frequency cosine components $x_2(t)$, an AM cosine component $x_3(t)$, and a Gaussian noise $s(t)$. The components' frequency is close to each other.

The sampling frequency is 2048 Hz, and the analysis points are 2048 points. The waveform and spectrum of $x(t)$ are shown in Figure 2. The spectrum basically shows each component. First, $x(t)$ is decomposed by the IVMD algorithm, and seven IMFs are extracted and shown in

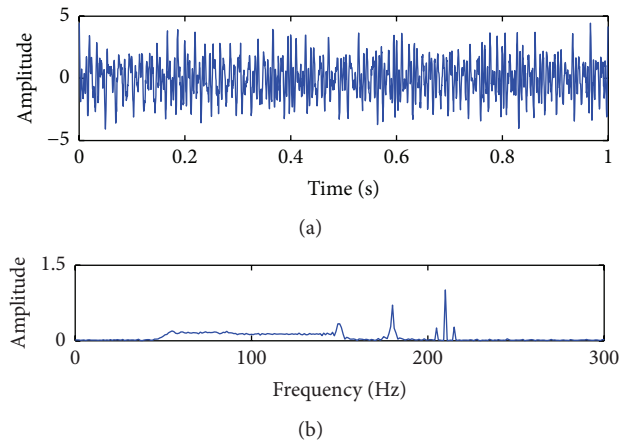


Figure 2: Simulation signal. (a) Waveform. (b) Fourier spectrum.

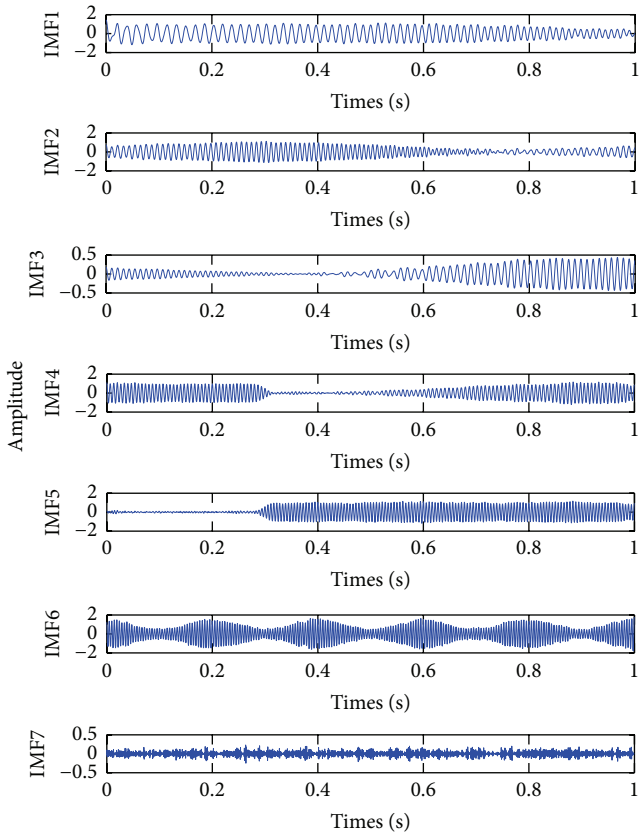


Figure 3: IMFs of simulation signal by IVMD.

Figure 3. IMF1~IMF3 are corresponding to $x_1(t)$, IMF4 and IMF5 are corresponding to $x_2(t)$, and IMF6 is corresponding to $x_3(t)$. The correlation coefficient between the IMFs and $x(t)$ is shown in Table 1. The former six IMFs are bigger than the threshold 0.05 and their time-frequency representations demodulated by TEO, respectively, are shown in Figure 4. It can be seen from Figure 4 that IVMD can effectively segregate the two FM components in $x_1(t)$, the mutation frequency at about 600th point in $x_2(t)$, and the AM component in $x_3(t)$.

Table 1: Correlation coefficient between IMFs and simulation signal.

| IMF1 | IMF2 | IMF3 | IMF4 | IMF5 | IMF6 | IMF7 |
|---|---|---|---|---|---|---|
| 0.5018 | 0.4726 | 0.3971 | 0.4480 | 0.4336 | 0.5266 | 0.0308 |

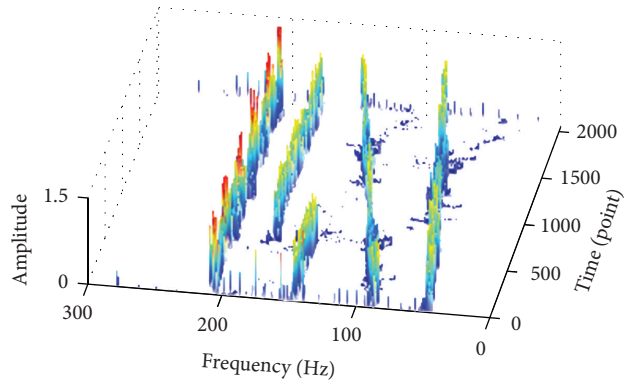


Figure 4: Time-frequency representation of simulation signal by IVMD-TEO.

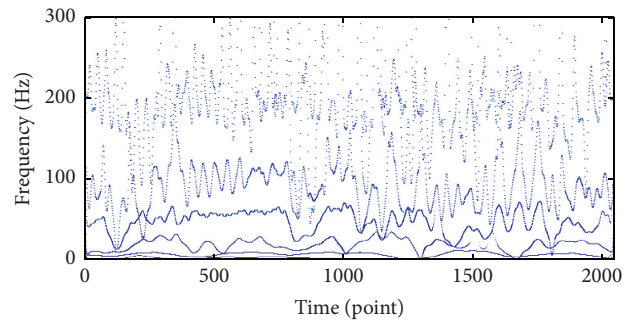


Figure 5: Time-frequency spectrum of simulation signal by HHT.

Although there is a little interference, all time-frequency representation of each component is clearly segregated.

For comparison, the time-frequency spectrum of simulation signal analyzed by the HHT is shown in Figure 5. It can be seen from Figure 5 that the frequency modulation phenomenon is confused. Two FM components in $x_1(t)$ are extracted partly, but the low disturbance frequency is emerged. There are frequency components in the vicinity of 200 Hz, but the detailed composition cannot be expressed. The analysis result is bad.

## 4. Experiment Rotor System Vibration Signal Analysis

The turbine rotor faults are simulated on the Bently RK-4 test rig (Figure 6). The test rig is an oil-fluid supporting rotor-bearing system. An electrical motor is attached to the shaft that carries two discs by a flexible coupling. A phase sensor closed to the coupling is fixed to measure the rotating speed. Two eddy current sensors, located near the rub copper thimble, are fixed by holder in the middle of test rig. A safety device is designed to ensure the experiment rotor safety. An

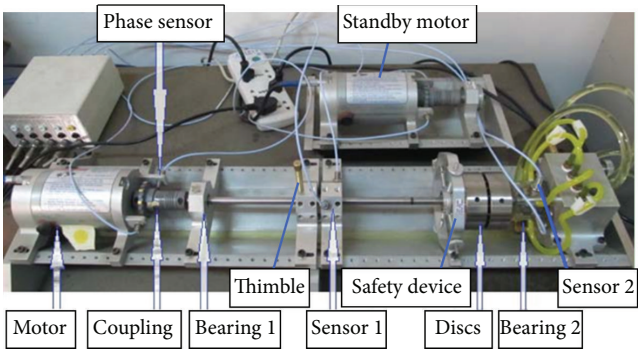


FIGURE 6: Rotor system test rig.

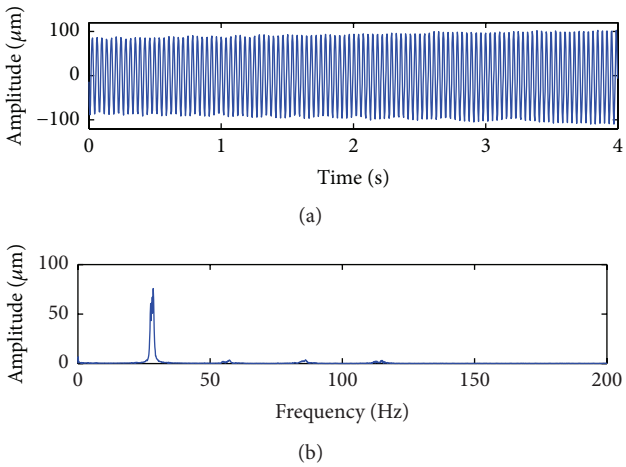


FIGURE 7: Rub-impact signal. (a) Waveform. (b) Fourier spectrum.

oil film journal bearing is part of an assembly connected to the oil pump system. The bearing is equipped with two proximity eddy current sensors in the horizontal and vertical directions. Rub-impact signal and oil film instability signal are gathered by sensor 1 and sensor 2, respectively using ZonicBook/618E vibration measurement system [6]. The sampling frequency is 5120 Hz. In order to reduce the amount of analysis data, the following analysis frequency is 512 Hz. That is to say, one point in ten is selected in sequence.

*4.1. Rub-Impact Fault Analysis.* The copper thimble that has a small separation from the shaft is fixed by holder in the middle of test rig and rubs against the high-speed rotating shaft slightly. The rub-impact signal when shaft speed is 1620 r/min~1740 r/min is analyzed and its waveform and spectrum are shown in Figure 7. The waveform amplitude becomes bigger with time, which only shows the rising rotational speed process. The spectrum only shows that the continuous rotational frequency is 27~29 Hz. It is difficult to diagnose the slight rub-impact fault accurately.

Seven IMFs obtained by IVMD for slight rub-impact signal are shown in Figure 8. In apparent periodicity components, IMF5 is corresponding to the rotational frequency ($1X$), IMF3 is corresponding to $2X$, IMF2 is corresponding to

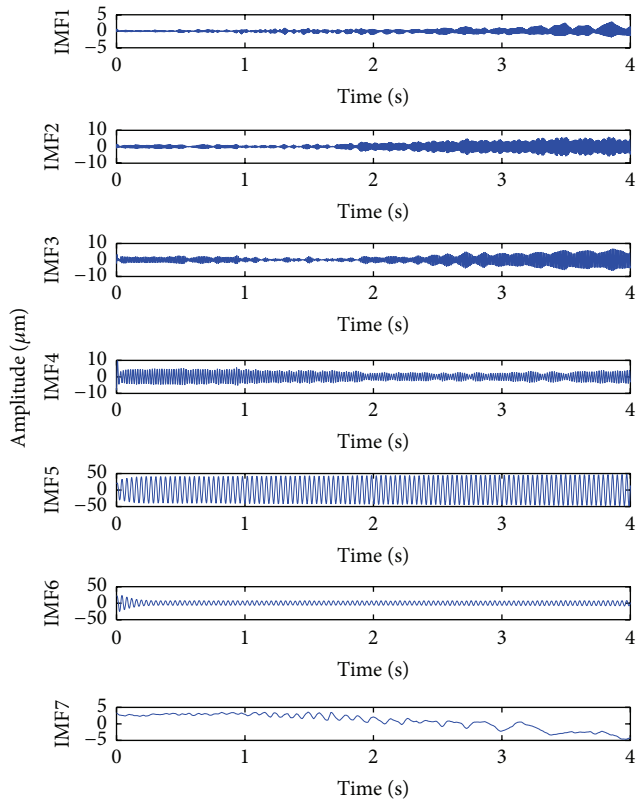


FIGURE 8: IMFs of rub-impact signal by IVMD.

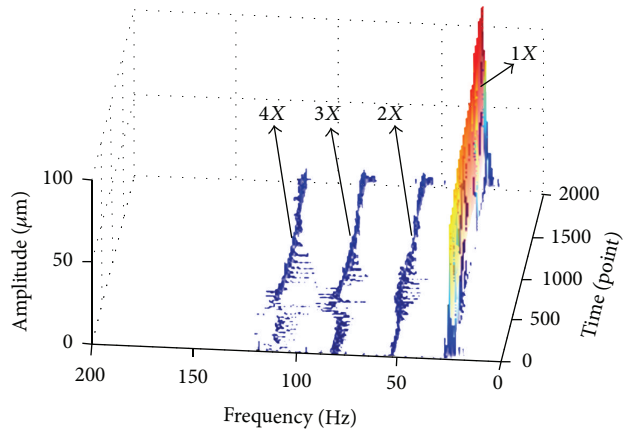


FIGURE 9: Time-frequency representation of rub-impact signal by IVMD-TEO.

$3X$, and IMF1 is corresponding to $4X$. The correlation coefficients of the former six IMFs are bigger than the threshold value. Their time-frequency representations demodulated by TEO are shown in Figure 9. It can be seen that the amplitude of rotational frequency is the maximum and $2X$~$4X$ frequency components are also extracted by IVMD-TEO. At the same time, the high harmonics frequency fluctuates in the range of 500th to 1000th point. It illustrates that the rub-impact process is instable. All of the frequency characteristics above accord with the rub-impact fault characteristics [25],

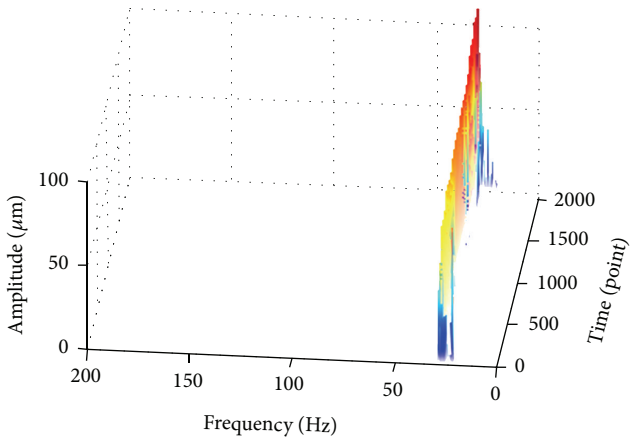


FIGURE 10: Time-frequency spectrum of rub-impact signal by HHT.

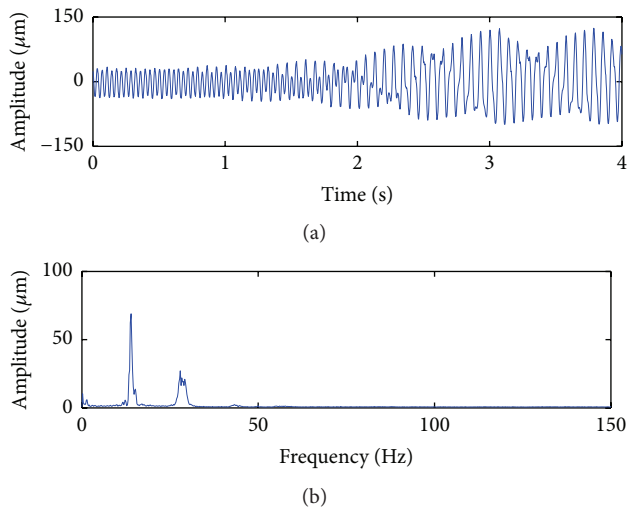


FIGURE 11: Oil-whirl signal. (a) Waveform. (b) Fourier spectrum.

so the occurrence of rotor slight rub-impact fault can be diagnosed accurately.

In order to compare the analysis results, the time-frequency analysis result for slight rub-impact signal by HHT is shown in Figure 10. It only shows demodulated rotational frequency and cannot show the high harmonics frequency. The slight rub-impact characteristics are not extracted. The analysis effect is not as good as the effect of IVMD-TEO.

*4.2. Oil Film Instability Analysis.* The oil film instability of the rotor system usually consists of two stages that are the nearly half speed oil-whirl and oil-whip. The monitor and control to initial oil-whirl are significant for turbine rotor to avoid great loss. The initial oil-whirl and the first-order oil-whip spectrum characteristics of the test rig are analyzed subsequently.

In the process of oil film instability, the oil-whirl occurs at the rising speed of 1620 r/min~1860 r/min, and the waveform and spectrum of the oil-whirl are shown in Figure 11. The rising speed can be seen in the waveform. In the spectrum, the

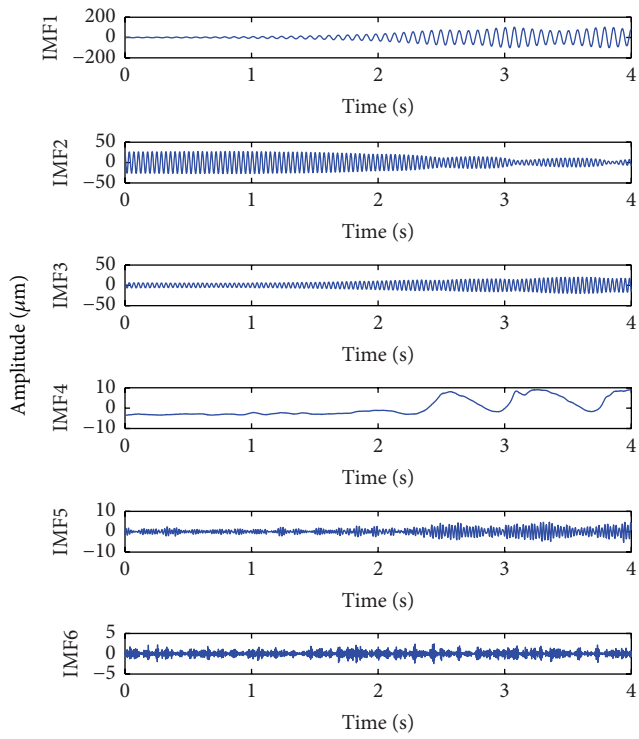


FIGURE 12: IMFs of oil-whirl signal by IVMD.

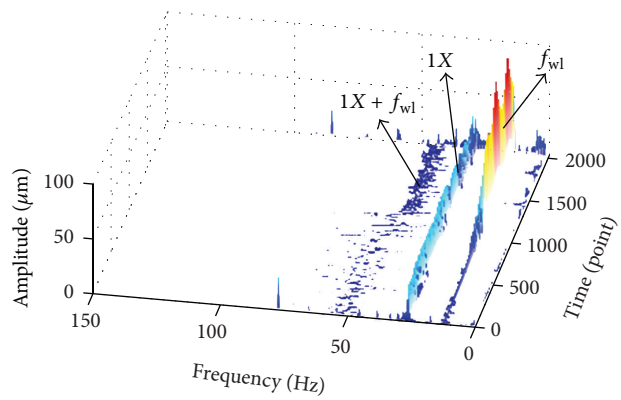


FIGURE 13: Time-frequency representation of oil-whirl signal by IVMD-TEO.

oil-whirl frequency ($f_{wl}$) (12~14 Hz) and 1$X$ (27~31 Hz) can be seen. The $f_{wl}$ value is about half value of 1$X$ and higher amplitude than 1$X$, but all of them lack the corresponding time information.

Six IMFs analyzed by IVMD to initial oil-whirl signal are shown in Figure 12. In apparent periodicity components, IMF1 is corresponding to $f_{wl}$. IMF2 and IMF3 are corresponding to 1$X$. The correlation coefficients of the former five IMFs are bigger than the threshold value. Their time-frequency representations demodulated by TEO, respectively, are shown in Figure 13. It can be seen that a little oil-whirl amplitude appears before 1000th point and the strong oil-whirl amplitude accompanied by amplitude modulation phenomenon appears after the 1000th point. The process

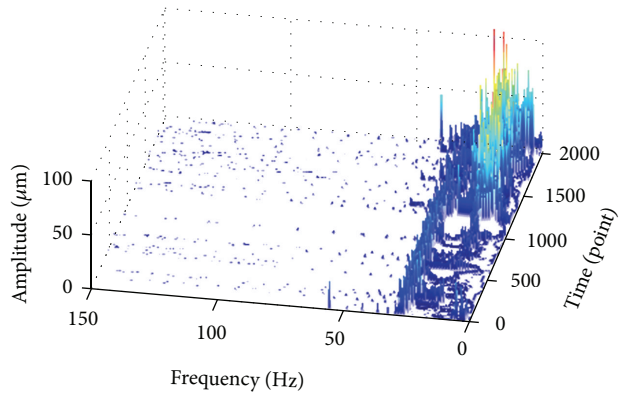


Figure 14: Time-frequency spectrum of oil-whirl signal by HHT.

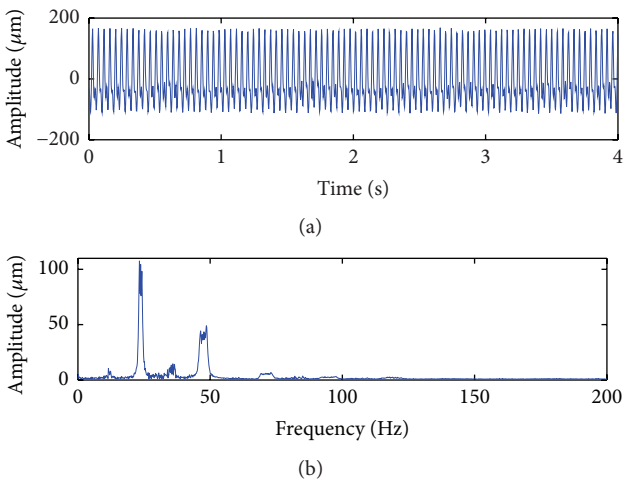


Figure 15: Oil-whip signal. (a) Waveform. (b) Fourier spectrum.

shows that the initial oil-whirl is instability process. The time-frequency representation clearly shows the whole process of the occurrence and development of oil-whirl. A phenomenon that a frequency component whose frequency is about $2X$ before the 1200th point and becomes $1X + f_{wl}$ after the 1200th point appears too. This detailed changing process suggests the high precision decomposition of IVMD-TEO.

For comparison, the time-frequency spectrum of oil-whirl signal analyzed by HHT is shown in Figure 14. The frequency mixing phenomenon is obvious, which cannot clearly show the whole process of the oil-whirl.

When the rotational speed is up to 2760 r/min~3000 r/min, the rotor system test rig shows biggish vibration because of the oil-whip. Waveform and spectrum of the oil-whip signal are shown in Figure 15. The rotational frequency ($1X$) (46~50 Hz) and the oil-whip frequency ($f_{wp}$) (22~24 Hz) can be seen in the spectrum, but they are continuous spectrum and lack corresponding time information. The oil-whip can be diagnosed preliminary.

Eleven IMFs obtained by IVMD to oil-whip signal are shown in Figure 16. The correlation coefficients of the former ten IMFs are bigger than the threshold value. Their time-frequency representations demodulated by TEO, respectively,

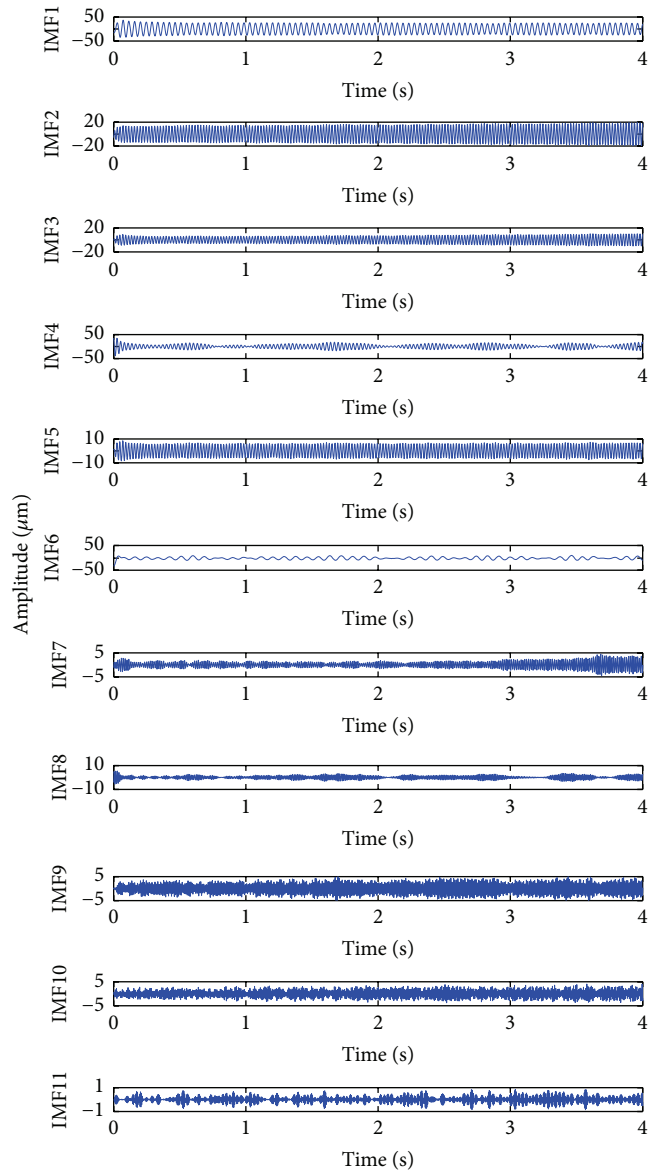


Figure 16: IMFs of oil-whip signal by IVMD.

are shown in Figure 17. Besides the main $1X$ and $f_{wp}$ frequency components, the related combination frequency components $f_{wp}/2$, $1X - f_{wp}/2$, $1X + f_{wp}$, $2X - f_{wp}/2$, $2X$, and $2X + f_{wp}$ are also extracted clearly. The oil-whip can be diagnosed accurately and reliably [25]. The analysis results also indicate the decomposition accuracy of the IVMD-TEO method.

To compare the analysis results, the time-frequency spectrum of oil-whip signal analyzed by HHT is shown in Figure 18. The $1X$, $f_{wp}$, and $f_{wp}/2$ frequency components are observed only and other frequency components cannot be extracted out. The analysis results are bad to IVMD-TEO method.

Qualitative analysis results in Figures 9, 13, and 17 for rotor faults show better effectiveness of the proposed method than HHT. The quantitative description in main fault

Table 2: Comparison of characteristic frequency average amplitude by HHT and IVMD-TEO.

| Rotor fault type | Fault frequency components (center frequency/Hz) | Extracted characteristic frequency average amplitude | | |
|---|---|---|---|---|
| | | HHT ($\mu$m) | IVMD-TEO ($\mu$m) | Improved ratio (%) |
| Rub-impact | $2X$ (56) | — | 3.88 | New |
| | $3X$ (84) | — | 4.13 | New |
| | $4X$ (112) | — | 3.50 | New |
| Oil-whirl | $f_{wl}$ (14) | 40.13 | 54.38 | 35.5 |
| | $1X$ (29) | 27.38 | 30.75 | 12.3 |
| | $1X + f_{wl}$ (43) | — | 3.38 | New |
| Oil-whip | $f_{wp}/2$ (11.5) | 3.50 | 4.25 | 21.4 |
| | $f_{wp}$ (23) | 88.13 | 99.25 | 12.6 |
| | $1X - f_{wp}/2$ (36.5) | — | 7.25 | New |
| | $1X$ (48) | 61.63 | 60.88 | −1.2 |
| | $1X + f_{wp}$ (71) | — | 5.88 | New |
| | $2X - f_{wp}/2$ (84.5) | — | 2.75 | New |
| | $2X$ (96) | — | 3.50 | New |
| | $2X + f_{wp}$ (119) | — | 3.13 | New |

Note: "—" represents no extracted fault frequency by HHT and "new" represents new extracted fault frequency by IVMD-TEO.

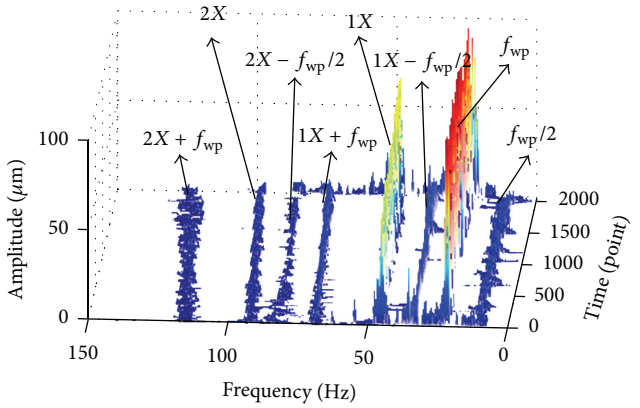


Figure 17: Time-frequency representation of oil-whip signal by IVMD-TEO.

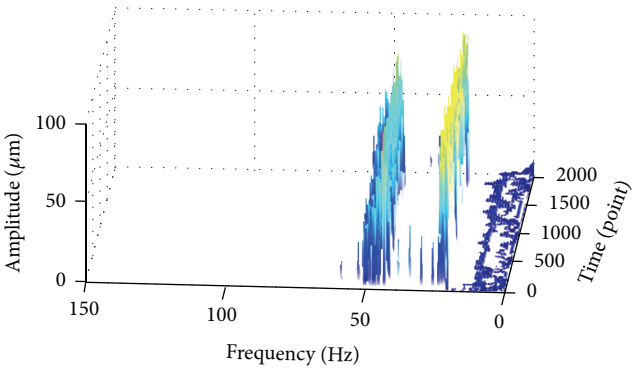


Figure 18: Time-frequency spectrum of oil-whip signal by HHT.

frequency amplitude's change and detailed fault frequency amplitude's value to every fault are shown in Table 2. For slight rub-impact fault, HHT method cannot extract fault frequency components; however, the proposed method can extract $2X$~$4X$ fault frequency components and their amplitudes are about 4 $\mu$m. For oil film instability fault (oil-whirl and oil-whip), most of the main fault frequency amplitudes extracted by proposed method, such as $1X$ oil-whirl, $f_{wl}$, and $f_{wp}$, are improved within 12.3%~35.5% comparing with HHT except $1X$ oil-whip frequency. The new extracted detail fault frequency amplitudes which cannot be extracted by HHT are also shown in Table 2. Both qualitative analysis and quantitative analysis can illustrate the advantage of IVMD-TEO method.

## 5. Conclusion

VMD is improved to determine the number of decomposition components adaptively using the correlation coefficient criterion. Integrating the advantages of IVMD and TEO, a time-frequency analysis method named IVMD-TEO is proposed in this paper. The analysis results of experimental turbine rotor signals under variable speed conditions illustrate that the method can show the time-frequency characteristics of slight rub-impact clearly, monitor the process of oil-whirl occurrence and development exactly, and extract the complicated time-frequency components of oil-whip accurately. It enhances the precision and accuracy of rotor fault diagnosis. Comparative analysis results show that the proposed method is more effective than HHT, so this method has important engineering application value for rotor fault diagnosis.

## Competing Interests

The authors declare that they have no competing interests.

## Acknowledgments

This work is supported by the National Natural Science Foundation of China (no. 51307058), the Natural Science Foundation of Hebei Province, China (nos. E2014502052

and E2015502013), and the Fundamental Research Funds for the Central Universities (nos. 2014MS156, 2015ZD27, and 2015XS120).

## References

[1] Y. Qin, "Multicomponent AM-FM demodulation based on energy separation and adaptive filtering," *Mechanical Systems and Signal Processing*, vol. 38, no. 2, pp. 440–459, 2013.

[2] C. Li and M. Liang, "Time-frequency signal analysis for gearbox fault diagnosis using a generalized synchrosqueezing transform," *Mechanical Systems and Signal Processing*, vol. 26, no. 1, pp. 205–217, 2012.

[3] Z. Feng, X. Chen, and M. Liang, "Iterative generalized synchrosqueezing transform for fault diagnosis of wind turbine planetary gearbox under nonstationary conditions," *Mechanical Systems and Signal Processing*, vol. 52-53, no. 1, pp. 360–375, 2015.

[4] Z. Feng, S. Qin, and M. Liang, "Time-frequency analysis based on vold-kalman filter and higher order energy separation for fault diagnosis of wind turbine planetary gearbox under nonstationary conditions," *Renewable Energy*, vol. 85, pp. 45–56, 2016.

[5] T. Ramesh Babu, S. Srikanth, and A. S. Sekhar, "Hilbert-Huang transform for detection and monitoring of crack in a transient rotor," *Mechanical Systems and Signal Processing*, vol. 22, no. 4, pp. 905–914, 2008.

[6] S. K. Liu, G. J. Tang, and B. Pang, "Rotor local rubbing fault feature analysis based on Teager-Huang transform," *Advanced Materials Research*, vol. 989–994, pp. 3244–3247, 2014.

[7] I. Antoniadou, G. Manson, W. J. Staszewski, T. Barszcz, and K. Worden, "A time-frequency analysis approach for condition monitoring of a wind turbine gearbox under varying load conditions," *Mechanical Systems and Signal Processing*, vol. 64-65, pp. 188–216, 2015.

[8] N. H. Chandra and A. S. Sekhar, "Fault detection in rotor bearing systems using time frequency techniques," *Mechanical Systems and Signal Processing*, vol. 72-73, pp. 105–133, 2016.

[9] Z. N. Li, M. Zhu, F. L. Chu, and Y. X. Xiao, "Mechanical fault diagnosis method based on empirical wavelet transform," *Journal of Scientific Instrument*, vol. 35, no. 11, pp. 2423–2432, 2014.

[10] G. Tang and B. Pang, "A mechanical fault diagnosis method based on improved Hilbert vibration decomposition," *Journal of Vibration and Shock*, vol. 34, no. 3, pp. 167–182, 2015.

[11] K. Dragomiretskiy and D. Zosso, "Variational mode decomposition," *IEEE Transactions on Signal Processing*, vol. 62, no. 3, pp. 531–544, 2014.

[12] G. Tang and X. Wang, "Parameter optimized variational mode decomposition method with application to incipient fault diagnosis of rolling bearing," *Journal of Xi'an Jiaotong University*, vol. 49, no. 5, pp. 73–81, 2015.

[13] C. Aneesh, S. Kumar, P. M. Hisham, and K. P. Soman, "Performance comparison of variational mode decomposition over empirical wavelet transform for the classification of power quality disturbances using support vector machine," *Procedia Computer Science*, vol. 46, pp. 372–380, 2015.

[14] Y. Wang, R. Markert, J. Xiang, and W. Zheng, "Research on variational mode decomposition and its application in detecting rub-impact fault of the rotor system," *Mechanical Systems and Signal Processing*, vol. 60, pp. 243–251, 2015.

[15] D. P. Bertsekas, "Constrained optimization and Lagrange Multiplier methods," in *Computer Science and Applied Mathematics* , vol. 1, Academic Press, Boston, Mass, USA, 1982.

[16] C. Someswara Rao and S. Viswanadha Raju, "Similarity analysis between chromosomes of Homo sapiens and monkeys with correlation coefficient, rank correlation coefficient and cosine similarity measures," *Genomics Data*, vol. 7, pp. 202–209, 2016.

[17] S. M. Zuurbier, S. Middeldorp, J. Stam, and J. M. Coutinho, "Sex differences in cerebral venous thrombosis: a systematic analysis of a shift over time," *International Journal of Stroke*, vol. 11, no. 2, pp. 164–170, 2016.

[18] Z. H. Zhao, S. P. Yang, and Y. J. Shen, "Machinery fault feature extraction based on independent component analysis and correlation coefficient," *Journal of Vibration and Shock*, vol. 5, no. 5, pp. 479–483, 2013.

[19] Z. Qiao and Z. Pan, "SVD principle analysis and fault diagnosis for bearings based on the correlation coefficient," *Measurement Science and Technology*, vol. 26, no. 8, Article ID 085014, 2015.

[20] M. Liang and I. S. Bozchalooi, "An energy operator approach to joint application of amplitude and frequency-demodulations for bearing fault detection," *Mechanical Systems and Signal Processing*, vol. 24, no. 5, pp. 1473–1494, 2010.

[21] P. Henríquez Rodríguez, J. B. Alonso, M. A. Ferrer, and C. M. Travieso, "Application of the Teager-Kaiser energy operator in bearing fault diagnosis," *ISA Transactions*, vol. 52, no. 2, pp. 278–284, 2013.

[22] X. Jiang, S. Li, and C. Cheng, "A novel method for adaptive multiresonance bands detection based on VMD and using MTEO to enhance rolling element bearing fault diagnosis," *Shock and Vibration*, vol. 2016, Article ID 8361289, 20 pages, 2016.

[23] P. Maragos, J. F. Kaiser, and T. F. Quatieri, "On amplitude and frequency demodulation using energy operators," *IEEE Transactions on Signal Processing*, vol. 41, no. 4, pp. 1532–1550, 1993.

[24] Y. Wang and R. Markert, "Filter bank property of variational mode decomposition and its applications," *Signal Processing*, vol. 120, pp. 509–521, 2016.

[25] H. Ma, T. Yu, Q. Han, Y. Zhang, B. Wen, and C. Xuelian, "Time-frequency features of two types of coupled rub-impact faults in rotor systems," *Journal of Sound and Vibration*, vol. 321, no. 3-5, pp. 1109–1128, 2009.